PERGAMON

International Journal of Plasticity
16 (2000) 1371–1390

INTERNATIONAL JOURNAL OF
Plasticity

www.elsevier.com/locate/ijplas

A multivariant micromechanical model for SMAs Part 2. Polycrystal model

Miinshiou Huang, Xiujie Gao *, L. Catherine Brinson

Department of Mechanical Engineering, Northwestern University, Evanston, IL 60208, USA

Received in final revised form 18 January 2000

Abstract

An averaging scheme is developed to simulate the behavior of a polycrystalline shape memory alloy (SMA) specimen using the Multivariant Micromechanics approach. An untextured polycrystalline specimen is assumed to be formed by a number of randomly oriented single crystal grains. The previously developed Multivariant technique is used to model the response of each single crystal grain subjected to its stress field seen in the polycrystalline sample. Using spherical grains, the Eshelby–Kröner approach is used to formulate the interaction between grains and to determine the stress state in each individual grain. This model successfully captures the basic features of SMA polycrystalline response to loading and temperature. In addition, comparison is made to recent experimental data with fully triaxial load states. Reasonable qualitative agreement is obtained and some issues related to crystallography of the material model are addressed.

Keywords: A. Microstructures; A. Phase transformation; A. Thermomechanical processes; B. Constitutive behaviour; B. Multiaxial loading

1. Introduction

With recent interest in the use of shape memory alloys (SMAs) as actuation elements in smart structures, as key components in medical devices and as the critical element in potential self-healing materials (Funakubo, 1987; Birman, 1997; Otsuka and Wayman, 1998), there is a great need to develop accurate models to describe shape memory material response to a variety of multiaxial load states. In previous

* Corresponding author.

0749-6419/00/$ - see front matter
PII: S0749-6419(00)00014-0

work (Huang and Brinson, 1998), we have developed a micromechanical model based on crystallographic variant information which can describe single crystal SMA response. As illustrated in Part 1 of this paper, retaining information on the crystallographic variants is important to obtain proper modeling response of the material, especially for complex thermo-mechanical loading.

Given these results illustrating the importance of accurately representing the crystallography at the single crystal level, here we extend the multivariant model to polycrystalline response. We believe that the results from this micromechanically based model will be insightful and could be used to verify and refine the assumptions that go into the transformation strain calculations in plasticity based approaches to SMA modeling (Graesser and Cozzarelli, 1994; Lagoudas et al., 1996; Auricchio and Taylor, 1997). As continued improvements are made to the single crystal model, as outlined in Part 1, the polycrystalline model as developed here will likewise become more accurate.

SMA models can be broadly classified into three categories: microscopic thermodynamics models, macroscopic phenomenological models, and micromechanics based macroscopic models. Microscopic thermodynamics models (Falk, 1983; Ball and James, 1987) are helpful for understanding the micro-scale behavior, such as nucleation, moving of the interface, and growth of a martensite plate, but are often difficult to apply for engineering level applications. Macroscopic phenomenological models (Liang and Rogers, 1990; Brinson, 1993; Graesser and Cozzarelli, 1994; Boyd and Lagoudas, 1996a,b; Lagoudas et al., 1996; Auricchio and Taylor, 1997; Bekker and Brinson, 1997) are generally more suitable for engineering applications due to their simplicity. However, most of the models in this group have been verified only for uniaxial loading. Even as macroscale multi-dimensional experimental data become available, we believe it is still very difficult to accurately represent general material response in a 3D phenomenological model without a good understanding of SMA response to complex loading at the microscale level.

Micromechanics based macroscopic models use thermodynamics laws to describe the transformation and utilize micromechanics to build up the material response based on the behavior of smaller subunits during transformation. For polycrystalline SMA models, micromechanics methods are used at two levels: first to assemble single crystal response based on variant formation and second to formulate polycrystal response based on an assembly of single crystal grains. Most of these models take the transformation strains of the martensitic variants into account, and some consider self-accommodation of variants, reorientation of variants, interaction of variants, and other features of martensitic transformation. Therefore, we believe this group of models is the most promising one to probe SMA response to complex stress states.

Among models in this group, we can further divide them into three subgroups: those that ignore both interaction between martensitic variants and interaction between grains (no-interaction models); those that ignore either the interaction between martensitic variants or interaction between grains (half-interaction models); and those that consider both interactions (full-interaction models). The multivariant polycrystalline model developed here is of the latter type: interaction between variants

is contained in the single crystal model and interactions between grains are included in the polycrystalline formulation.

A simple Reuss approximation (Mura, 1987) for polycrystal response would belong to the no-interaction group if it does not account for interaction between variants at all (no such model has been proposed). In this paper a Reuss approximation is used at the polycrystal level for comparison to the full-interaction model developed here. The Reuss approximation in this context is a half-interaction model since the single crystal (individual grain) response is calculated with the multivariant model which accounts for interaction between variants. The model used by Gall et al. (1998) is also considered as a half-interaction model because there is no interaction between variants, but grains do interact by using the self-consistent method. Both models proposed by Lexcellent et al. (1996) and Vivet and Lexcellent (1998) belong to the half-interaction group because only one variant is available in each grain, therefore no interaction exists among variants. Sun and Hwang's model (1991, 1993a,b) also belongs to the half-interaction group since no variants are considered in the model. Patoor et al. (1994) proposed a model which almost accounts for both interactions. The interaction between variants is partially considered since a simplified interaction matrix was used to formulate the interaction energy instead of using the Eshelby–Kröner approach. Lu and Weng's (1997, 1998) model was developed from the previous one and thus belongs to half-interaction group as well.

One critical shortfall among the models mentioned above is that the interaction between variants is ignored or only partially considered. While all of the models account for intergrain interactions, we believe that the variant interactions are important even in polycrystal models since the latter allow switching of variants during martensitic transformation under complex temperature and stresses paths. The results here will show that crystallographic details important for single crystal response (as seen in Part 1) still significantly impact polycrystal results.

In the following we will first develop the polycrystalline model theory in Section 2 and show basic results of the simulations in Section 3. In Section 4 we will compare to some data from the literature for a SMA subjected to triaxial loading and discuss implications of the results for continued model improvements.

2. Polycrystal model based on micromechanics

The behavior of single and polycrystalline SMAs are quite different. As we have seen in Part 1, the single crystal SMAs are highly anisotropic and this fact has serious implications in both the modeling and experimental response. An untextured polycrystalline material, however, consists of many single crystal grains randomly oriented, leading to an overall isotropic response. In addition, the transformation and stress–strain curves of single crystal specimens have sharp corners where transformation initiates and finishes, representing abrupt initiation of transformation at certain critical stresses/temperatures. For a polycrystalline SMA specimen, while local strain measurements can demonstrate abrupt transformation under certain

conditions (Shaw and Kyriakides, 1995), global stress–strain response typically occurs more gradually in a transformation zone of stress or temperature.

In this section, simulation of a polycrystalline specimen will be conducted by assuming that a number of randomly oriented single crystal grains are in the polycrystalline specimen (Fig. 1) and the single crystal model developed will be used in each single crystal grain. A self-consistent method (Kröner, 1961; Budiansky and Wu, 1962; Goo and C, 1997) is used to calculate the average internal stress of each grain. With a similar technique, it is straightforward to represent textured materials by assigning appropriate non-random grain orientations.

In a polycrystalline material, the transformation strains differ between grains and all grains interact with each other due to the incompatibility of these different transformation strains. As a consequence, the average stresses in each grain also differ. To determine the average stress in each grain a self-consistent method is used. The actual transformation strain in grain γ is $\varepsilon_{ij}^{\gamma}$, which is

$$\varepsilon_{ij}^{\gamma} = \sum_{n=1}^{N_{\text{var}}} f^n \varepsilon_{ij}^n \tag{1}$$

where N_{var} is the number of variants (same as N in single crystal case). If all grains have the same transformation strain, the stress due to the incompatibility of transformation strain is zero. To utilize the Eshelby's solution, we assume that the difference between the actual transformation strain of each grain and the average

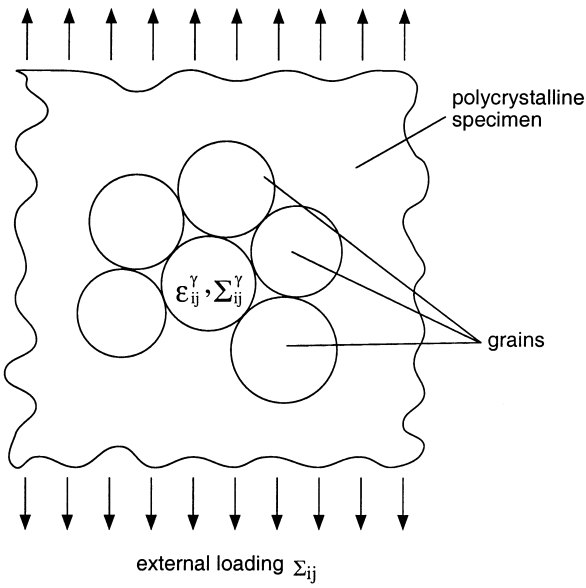

Fig. 1. Polycrystalline specimen is modeled as a number of random-oriented, spherical, single-crystalline grains.

transformation strain is the "effective transformation strain" or eigenstrain. Thus, the effective transformation strain in grain γ is $\hat{\varepsilon}_{ij}^{\gamma}$:

$$\hat{\varepsilon}_{ij}^{\gamma} = \varepsilon_{ij}^{\gamma} - \frac{1}{N_{\text{grain}}} \sum_{n=1}^{N_{\text{grain}}} \varepsilon_{ij}^{n} \tag{2}$$

where N_{grain} is the number of grains. The stress in grain γ due to incompatibility with other grains can be calculated by using Eshelby's solution.

$$\hat{\sigma}_{ij}^{\gamma} = C_{ijkl}(S_{klmn}\hat{\varepsilon}_{mn}^{\gamma} - \hat{\varepsilon}_{kl}^{\gamma}) \tag{3}$$

where S_{klmn} is the Eshelby tensor of spherical inclusion. The average stress in grain γ is the summation of external stress and the stress due to incompatibility, that is

$$\Sigma_{ij}^{\gamma} = \Sigma_{ij} + \hat{\sigma}_{ij}^{\gamma} \tag{4}$$

In the following sections, a 10-grain specimen will be used to simulate a polycrystalline material. These grains are randomly oriented to avoid texture effect in the material. The orientation of each grain is decided by three random Euler angles. For example, for grain γ, the three random Euler angles are $(\phi^{\gamma}, \theta^{\gamma}, \psi^{\gamma})$, where ϕ^{γ} is a rotation w.r.t. axis x_3, θ^{γ} is a rotation w.r.t. axis x_2, and ψ^{γ} is a rotation w.r.t. axis x_3 again. The transformation matrices for these three angles are

$$R^3(\varphi^{\gamma}) = \begin{bmatrix} \cos\varphi^{\gamma} & -\sin\varphi^{\gamma} & 0 \\ \sin\varphi^{\gamma} & \cos\varphi^{\gamma} & 0 \\ 0 & 0 & 1 \end{bmatrix} \tag{5}$$

$$R^2(\theta^{\gamma}) = \begin{bmatrix} \cos\theta^{\gamma} & 0 & \sin\theta^{\gamma} \\ 0 & 1 & 0 \\ -\sin\theta^{\gamma} & 0 & \cos\theta^{\gamma} \end{bmatrix} \tag{6}$$

$$R^3(\psi^{\gamma}) = \begin{bmatrix} \cos\psi^{\gamma} & -\sin\psi^{\gamma} & 0 \\ \sin\psi^{\gamma} & \cos\psi^{\gamma} & 0 \\ 0 & 0 & 1 \end{bmatrix} \tag{7}$$

The combined transformation matrix, R^{γ}, is

$$R^3(\psi^{\gamma})R^2(\theta^{\gamma})R^3(\varphi^{\gamma}) \tag{8}$$

The transformation strain after rotation for variant n in grain γ can be obtained by

$$\{\varepsilon_{ij}^{n}\}^{\gamma} = R^{\gamma}\{\varepsilon_{ij}^{n}\}R^{\gamma T} \tag{9}$$

where $\{\varepsilon_{ij}^{n}\}$ is the transformation strain of variant n in grain γ before rotation, and $R^{\gamma T}$ is the transpose matrix of R^{γ}. The physical meaning of the rotation is that the

material is rotated by an angle ϕ with respect to axis x_3 of the space coordinate system, and then by an angle θ with respect to axis x_2, and finally by an angle ψ with respect to x_3 again.

The multivariant polycrystalline response is calculated numerically, incrementing the load and iterating to solution at each step. In each loading step, the program checks each grain for nonbalanced driving forces; if it finds a nonbalanced grain, it calculates the new volume fractions of each variant in that grain by a single Runge–Kutta step. After all the grains are checked and the new martensite fractions for nonbalanced grains are obtained, the program uses the new martensite fraction of each variant in each grain to calculate the stresses in each grain by using (1)–(4). Then the program checks all grains, advances the non-balanced grains for one Runge–Kutta step, and then recalculates the stresses in each grain again, repeating until all grains are balanced.

In the following, 10 grain samples are used for most of the results for speed of computation. In one case a comparison between 10 and 100 grain samples is made, illustrating that changes in overall response between the two cases is subtle.

3. Basic results for polycrystalline SMAs

Two different CuZnAl SMA materials are used in Part 2 and the parameters we used for them are listed in Table 1a in Part 1. One set of crystallographic data for $Cu_{75}Zn_{17}Al_8$ (wt.%) was determined by Saburi and Wayman (1979) and the lattice parameters of it were measured by Chakravorty and Wayman (1977). Another set of crystallographic data for $Cu_{70}Zn_{26}Al_4$ (wt.%) were recalculated by the authors using the lattice parameters measured by Zhu et al. (1986). Both alloys demonstrate negative volume change of $\Delta v/v \approx -0.36\%$ (Patoor et al., 1995) and -0.17% (Zhu et al., 1986) respectively. The transformation strains for $Cu_{75}Zn_{17}Al_8$ (wt.%) were given in Table 1b in Part 1 of this paper and are not repeated here. Unless explicitly mentioned all the calculation in Part 2 are using the parameters in Table 1b in Part 1. Here we first examine the standard, baseline SMA responses for the polycrystalline model before considering a more complex loading example in Section 4.

3.1. Temperature induced transformation

Fig. 2 shows the prediction by this model using a 10-grain polycrystalline SMA. The model predicts a sudden transformation from the parent phase to martensite and a gradual transformation from martensite to the parent phase, that is $M_s = M_f$, but $A_f > A_s$. The reason for the sharp forward transformation and gradual reverse transformation is that during the forward transformation process, before the transformation starts, the material is in the parent phase for all grains. There is no distinction between grains for temperature change and all grains will transform at the same temperature. After the material transforms to different variants of martensite in each grain, there are different stresses produced in each grain because of the

Table 1
Uniaxial (1 and 3) and 3D (2 and 4–7) stress state applied to the polycrystalline CuZnAl specimens

Test number and description	Applied stress state	Effective stress σ_{eff}	Relative hydrostatic pressure σ_{h}
# 1 Pure tension	$\sigma_{ij} = \begin{bmatrix} \sigma & 0 & 0 \\ 0 & 0 & 0 \\ 0 & 0 & 0 \end{bmatrix}$	σ	$+0.33\sigma_{\text{eff}}$
# 2 Zero hydrostatic stress	$\sigma_{ij} = \begin{bmatrix} 2\sigma & 0 & 0 \\ 0 & -\sigma & 0 \\ 0 & 0 & -\sigma \end{bmatrix}$	3σ	$-0.00\sigma_{\text{eff}}$
# 3 Pure compression	$\sigma_{ij} = \begin{bmatrix} -\sigma & 0 & 0 \\ 0 & 0 & 0 \\ 0 & 0 & 0 \end{bmatrix}$	σ	$-0.33\sigma_{\text{eff}}$
# 4 Triaxial compression	$\sigma_{ij} = \begin{bmatrix} -3\sigma & 0 & 0 \\ 0 & -\sigma & 0 \\ 0 & 0 & -\sigma \end{bmatrix}$	2σ	$-0.83\sigma_{\text{eff}}$
# 5 Triaxial compression	$\sigma_{ij} = \begin{bmatrix} -2\sigma & 0 & 0 \\ 0 & -\sigma & 0 \\ 0 & 0 & -\sigma \end{bmatrix}$	σ	$-1.33\sigma_{\text{eff}}$
# 6 Triaxial compression	$\sigma_{ij} = \begin{bmatrix} -1.7\sigma & 0 & 0 \\ 0 & -\sigma & 0 \\ 0 & 0 & -\sigma \end{bmatrix}$	0.7σ	$-1.76\sigma_{\text{eff}}$
# 7 Pure hydrostatic stress	$\sigma_{ij} = \begin{bmatrix} -\sigma & 0 & 0 \\ 0 & -\sigma & 0 \\ 0 & 0 & -\sigma \end{bmatrix}$	0	$-\infty\sigma_{\text{eff}}$

interaction between them. So the grains will transform back to parent phase at different temperatures.

Although exact measurements of the continuous evolution of volume fraction of a SMA with temperature change are rare, transformation temperatures corresponding to the beginning and end of transformation are readily obtained by DSC measurements. Such results typically show much wider ranges of transformation, often on the order of 10 degrees between M_s and M_f for example. The current model does not predict this range for temperature induced transformations; however, incorporation of the latent heat of transformation into the model predictions would enable us to capture this feature. As we focus more on temperature effects in future work, heat of transformation will need to be included.

3.2. Pseudoelasticity

The stress–strain curves by shearing ($\Sigma_{12} \neq 0$, all other $\Sigma_{ij} = 0$) of a 10-grain and a 100-grain poly-crystalline specimen at temperature $T = T_0 + 25^{\circ}\text{K}$ are given in

Fig. 3. One sees that the 100-grain case has lower forward and higher backward transformation plateau stresses. This is expected since more grains with lower (higher) forward (backward) transformation stresses are available in the 100 grain case. Another slight difference is the slope of unloading curve. Although two curves differ somewhat as mentioned, both curves exhibit the same basic features. Since the complete stress-strain curve for 100-grain case requires longer to calculate, we will

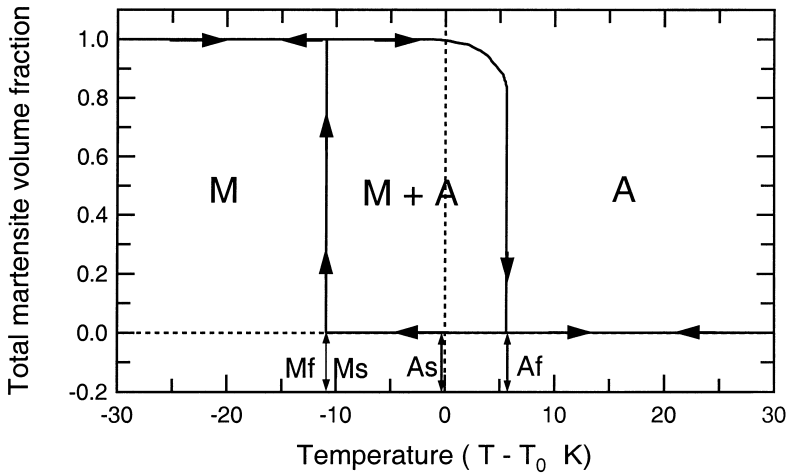

Fig. 2. Total martensite volume fraction vs. temperature for a temperature induced martensite transformation predicted by a 10-grain polycrystalline SMA.

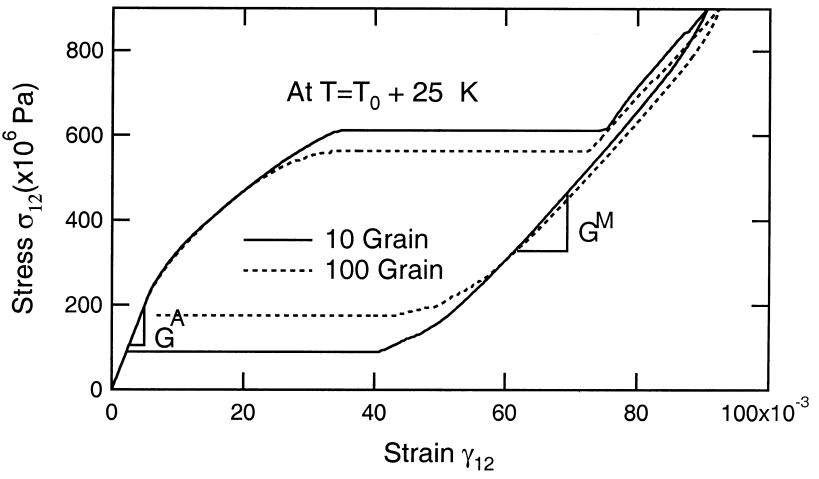

Fig. 3. Pseudoelasticity stress–strain curve for a 10-grain and a 100-grain polycrystalline specimen ($T = T_0 + 25°\mathrm{K}$).

use the 10 grain case for the remaining examples. Fig. 3 illustrates that the 10-grain simulation can capture the important attributes of the material response as well as a 100-grain case.

The stress–strain curves in Fig. 3 show several characteristics of this model: The first feature is that forward and reverse transformations of the poly-crystalline material specimen do not occur at a fixed stress as in the single crystal case. Here, the transformation occurs very slowly at first, beginning at ~220 MPa. As the stress is gradually increased, the transformation accelerates, and at a certain stress transformation is suddenly completed (at ~550 MPa for the 100 grain case). The gradual then accelerating transformation is due to the differing transformation stresses in each grain and the stress interactions between grains. When the stress reaches the lowest critical transformation stress, the grain with the lowest critical transformation stress will start to transform. The grain which starts to transform will become softer and carry less load, so that other grains sustain more load, which in turn causes remaining grains to transform faster. Fig. 4 shows the stress and transformation strain of each grain, as well as the overall stress and transformation strain. We can see that the microscopic transformation stress range (the highest stress needed to fully transform one of the grains minus the lowest starting transformation stress among all the grains) is about 730 MPa in this case, but the macroscopic transformation stress range is only about 370 MPa.

The second feature of the model is that although the elastic moduli at the single crystal level are assumed to be the same for both martensite and the parent phase, the slopes of the polycrystalline stress–strain curve in Fig. 3 representing austenitic modulus (loading) and martensitic modulus (unloading) are different. The phenomenon of different apparent moduli for different phases can be seen in experimental

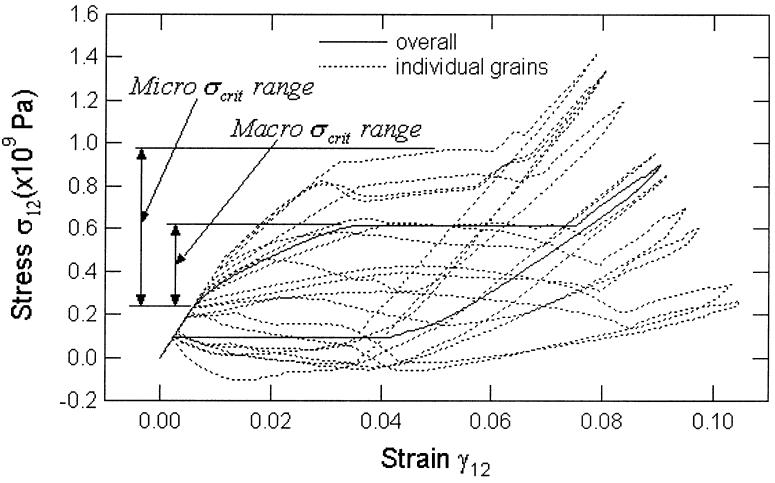

Fig. 4. Stress–strain curve of overall specimen and individual grains for PE of 10-grain specimen.

data on polycrystals (Funakubo, 1987; Brinson, 1993; Shaw and Kyriakides, 1995). Most macroscopic phenomenological models assume different moduli for martensite and the parent phase, but this result shows that it is possible to capture this phenomenon by assuming same moduli for both phases at the single crystal level. What happens here is that even with the martensite transformation complete, the changing stress causes the material to switch between different variants, resulting in a slope change for the overall specimen response.

Note that in our model, we are simulating switching of habit plane variants (HPVs) only. To better represent actual material response, consideration of the internally twinned structure should be added. For example, in martensitic structures such as 2H, each habit plane variant is composed of two correspondence variants (CVs). Switching upon loading has been experimentally observed among correspondence variants through the twinning mechanism (Saburi and Nenno, 1981). For structures such as 18R, while each HPV is composed of only one CV (with stacking faults for accommodation), Saburi et al. (1980), and Saburi and Nenno (1981)) reported that switching among CVs also occurs by twinning. In both cases, it has been seen that the twinning/switching during loading can occur even between two CVs not in the same self-accommodated group. How to appropriately model CV twinning will be further addressed in future work.

Another visible feature of Fig. 3 is that during unloading, the curve is not straight. In most experiments, the unloading curves are not straight (Funakubo, 1987; Shaw and Kyriakides, 1995; Fremond and Miyazaki, 1996), but yet no macroscopic phenomenological models have considered this effect. The multivariant model captures this macroscopic feature by the switching of variants (HPVs) in each single crystal grain during unloading. The model predicts variant switching during unloading, at first gradual, then increasing as the load continues to decrease until the true reverse transformation to austenite begins. The effect of variant switching and reverse transformation blend together making a very rounded corner on the stress–strain curve.

3.3. Shape memory effect

Fig. 5 shows the stress–strain curve of a 10-grain polycrystalline specimen at temperature $T = T_0$. The forward transformation is essentially the same as the forward transformation in the pseudoelasticity. Here a second yielding is observed when the stress continues to increase after the transformation finishes. Some tensile test data for SMAs show such a second yielding (Otsuka et al., 1979; Funakubo, 1987), but there is not much discussion of this phenomena yet. In this example prediction from the model, the second yielding is interpreted as fast switching to different variants with a larger possible transformation strain.

Upon unloading, the slow switching of martensite variants also occurs as in pseudoelasticity resulting in the nonlinear unloading curve, but because of the lower temperature there is no reverse transformation. When heated the material starts to transform back to parent phase at the temperature about ($T_0 + 5.4^\circ$K) and finishes at about ($T_0 + 16.2^\circ$K).

3.4. Reuss approximation for polycrystalline SMAs

It is illustrative to compare the polycrystalline model developed here with a much simpler Reuss approximation. In both cases, we will use the single crystal Multivariant model for the response of each grain.

The Reuss approximation (Mura, 1987), typically used for the average elastic moduli of composite materials, assumes that all the elements of a composite material are subjected to a uniform stress equal to the average applied stress. We can apply this simple method also to determine a quick estimate of a polycrystalline SMA response. Here we then assume that the stress in each grain of a polycrystal is the same as the average stress applied to the polycrystal as in Fig. 6. Note that this provides a half-interaction type prediction of material response, according to our earlier classification, since the response of one grain does not impact the stress or strain state in the neighboring grain.

Again we will use 10 randomly oriented grains to represent non-textured and isotropic behavior of a shape memory alloy specimen. For the Reuss Approximation each of the grains was simulated using the single crystal model with the stress equal to the applied macroscopic stress providing the result of $\bar{\varepsilon}^r_{ij}$ as the average macroscopic

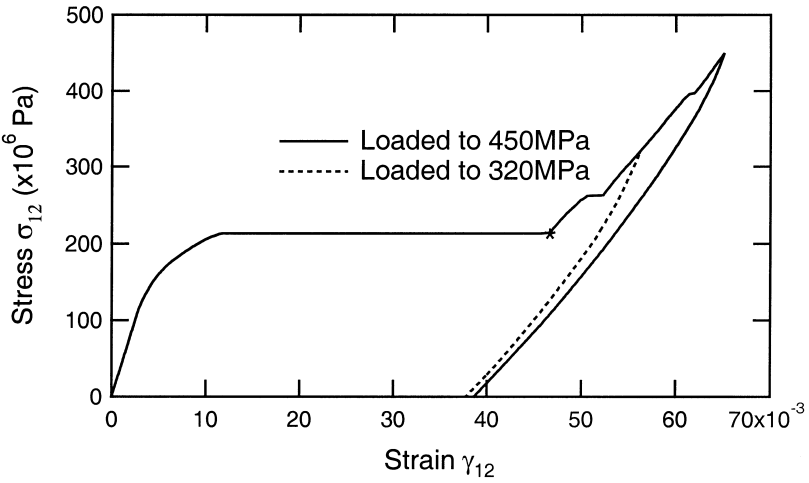

Fig. 5. Stress–strain curve of a 10-grain polycrystalline specimen at temperature $T = T_0$ predicted by the model. *, forward transformation to 100% martensite.

Fig. 6. Schematic drawing of applying stress on a polycrystalline specimen containing 10 randomly oriented grains.

strain of the rth grain. The average macroscopic strain of the polycrystal was calculated using

$$\bar{\varepsilon}_{ij} = \sum_{r=1}^{n} C_r \bar{\varepsilon}_{ij}^{r} \tag{10}$$

where C_r is the volume fraction of grain r and n is the number of grains. Since all grains are equally weighted, C_r is simply equal to 1/n and $\bar{\varepsilon}_{ij}$ can be simplified to

$$\bar{\varepsilon}_{ij} = \frac{1}{n} \sum_{r=1}^{n} \bar{\varepsilon}_{ij}^{r} \tag{11}$$

The result of shape memory effect under uniaxial tension using the full-interaction polycrystalline model of the previous section is shown in Fig. 7 along with that predicted by the Reuss approximation. The stress strain curve for the grains having the lowest and highest transformation stresses are also given. Note that the stress at which transformation first begins is same for both polycrystalline predictions. This result is expected since the macroscopic stress in each model is same and there is no transformation induced stress (stress due to incompatibility) in the full-interaction model until the first grain begins transformation. Thus both models start transformation in the same grain at the same stress level. The ultimate stress levels achieved for the two models are also similar, however the Reuss shows a multi-stage transformation while the full-interaction model has variant switching after full transformation.

The most obvious difference between the $\sigma-\varepsilon$ curves for the two models is that the Reuss approximation results in twice as much strain as the full-interaction model.

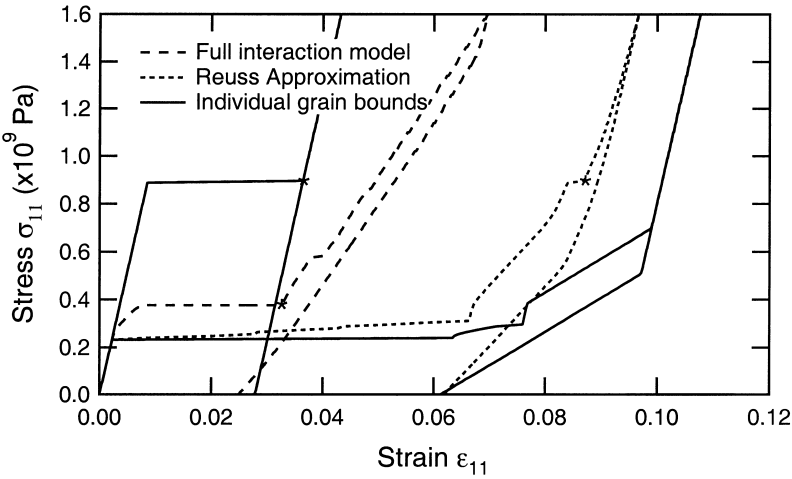

Fig. 7. Stress–strain curves predicted by both Reuss approximation and polycrystal model for a 10-grain polycrystalline specimen. Forward transformation to 100% martensite is indicated by * on each curve.

This phenomenon can be accounted for by considering the relationship between orientation and macroscopic strain. Since each grain has a different orientation, its final macroscopic strain under the same uniaxial tension is different. Some grains are favorably oriented to the applied uniaxial tension and thus exhibit larger macroscopic distortion. In the Reuss approximation, each grain behaves independently, i.e. no restriction or interaction between grains. Therefore those favorably oriented grains which give large transformation strain were fully strained and contribute greatly to the average strain. In the full-interaction model, however, the interaction among grains plays an important role. In order to maintain compatibility among grains, those grains which could exhibit a large transformation strain are restrained by neighboring grains resulting in a much lower overall strain.

4. Comparison to experiments

In this section, triaxial loading simulation results predicted by our model for two CuZnAl materials (mentioned in Section 3) are compared to the experimental results by Gall et al. (1998) on a polycrystalline SMA. One dimensional tensile and compressive simulation and experimental results are also discussed here to amplify discussion of hydrostatic pressure effects on the transformation stresses.

There are only a few triaxial loading experiments which have been performed to investigate the effect of three dimensional stress states on martensitic transfromation in SMAs. Jacobus et al. (1996) investigated the effects of triaxial loading in a polycrystalline Ni–Ti SMA. Lim and McDowell (1999) investigated the response of a Ni–Ti SMA specimen under axial-torsional proportional and nonproportional loading. Recently, Gall et al. (1998) investigated these effects in a polycrystalline $Cu_{71}Zn_{25}Al_4$ (wt.%) SMA with a negative volume change of $\Delta v/v \approx -0.3\%$. Under uniaxial loading, it was found that the compressive stress level required to macroscopically trigger the transformation was 34% larger than the required tensile stress. The triaxial tests produced effective stress–strain curves with critical transformation stress levels in between the tensile and compressive results.

The effective stress–strain plots above A_f under a loading rate of $\mathrm{d}s/\mathrm{d}t = 10^{-4}$ s are shown in Fig. 8. Curves for the effective stress at the onset of transformation vs. the hydrostatic stress at the onset of transformation above A_f are shown in Fig. 9. The effective stress and effective strain are calculated by:

$$\sigma_{\text{eff}} = \frac{\sqrt{2}}{2}[(\sigma_{11} - \sigma_{22})^2 + (\sigma_{11} - \sigma_{33})^2 + (\sigma_{22} - \sigma_{33})^2]^{1/2} \tag{12}$$

$$\varepsilon_{\text{eff}} = \frac{\sqrt{2}}{3}[(\varepsilon_{11} - \varepsilon_{22})^2 + (\varepsilon_{11} - \varepsilon_{33})^2 + (\varepsilon_{22} - \varepsilon_{33})^2]^{1/2} \tag{13}$$

where σ_{nn} and ε_{nn} are the nth principal stress and strain respectively. For the tests in Fig. 8 and 9 the applied stress state, the effective stress and the relative hydrostatic pressure are shown in Table 1.

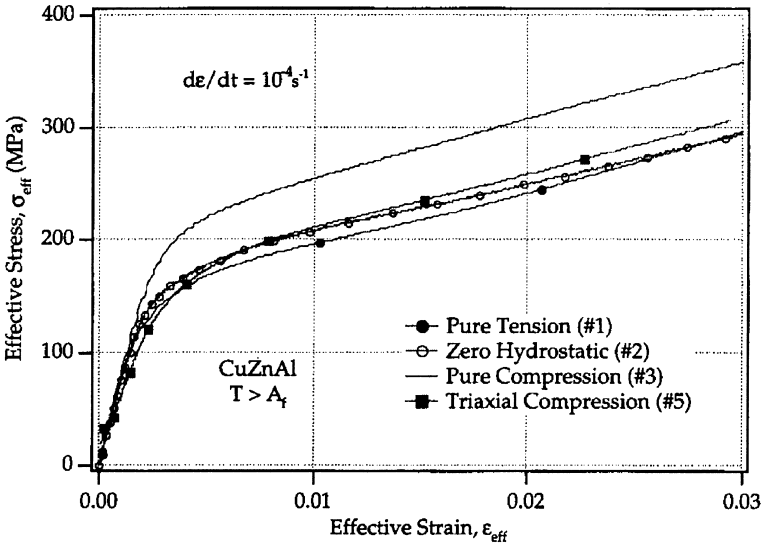

Fig. 8. Effective stress–strain plots for a polycrystalline CuZnAl SMA specimen above A_f. Each one of the curves corresponds to a 1D or 3D loading (after Gall et al., 1998).

Using the crystallographic data of these two CuZnAl alloys (mentioned in Section 3), we simulated all the one dimensional and three dimensional loading paths listed in Table 1. The effective stress–strain curves for $Cu_{75}Zn_{17}Al_8$ (wt.%) similar to Fig. 8 are plotted in Fig. 10. The effective stress at the onset of transformation vs. the hydrostatic stress at the onset of transformation similar to Fig. 9 for both $Cu_{75}Zn_{17}Al_8$ (wt.%) and $Cu_{70}Zn_{26}Al_4$ (wt.%) are shown in Fig. 11.

At first glance, the experimental curves in Fig. 8 and the polycrystal model curves in Fig. 10 look similar. In all loading cases there is a narrow transition zone before rapid transformation to oriented martensite. Also, in both experiment and model there is a modest difference of 100–150 MPa in the values of the transformation stresses for the different loading cases. Upon closer inspection, however, there are a number of differences between the experimental results and the model predictions. First, the strain hardening during transformation seen in the experimental results is not reflected in the model. We believe this discrepancy is due to the model's use of isotropic moduli for both martensite and austenite. As discussed in Part 1 of this paper, crystallographic data indicates that while austenite is highly anisotropic, the martensitic phase has a lower anisotropy factor (Guenin et al., 1980). If this anisotropy were properly incorporated into the model it could impart a strain hardening result upon transformation. In addition, the magnitudes of the transformation stresses are about 50% too high in the model predictions of Fig. 10: again we believe that anisotropy of the phases could be key to properly capturing transformation stress levels. As shown in Part 1 of this paper, changing the modulus of the material greatly reduces predicted transformation stresses. For the polycrystalline model, with some grains oriented in a "weaker" direction to the applied loading, their

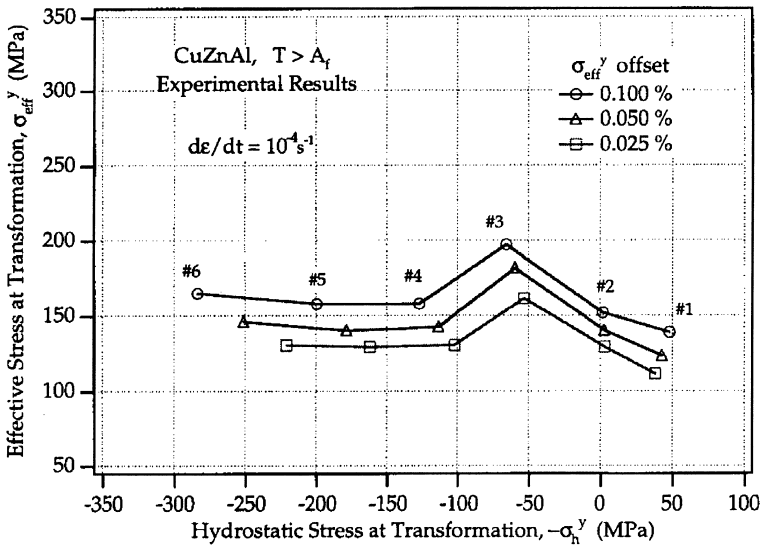

Fig. 9. Effective stress at the onset of transformation vs. the hydrostatic stress at the onset of transformation for a polycrystalline CuZnAl SMA specimen above A_f. Each number corresponds to a 1D or 3D loading (after Gall et al., 1998).

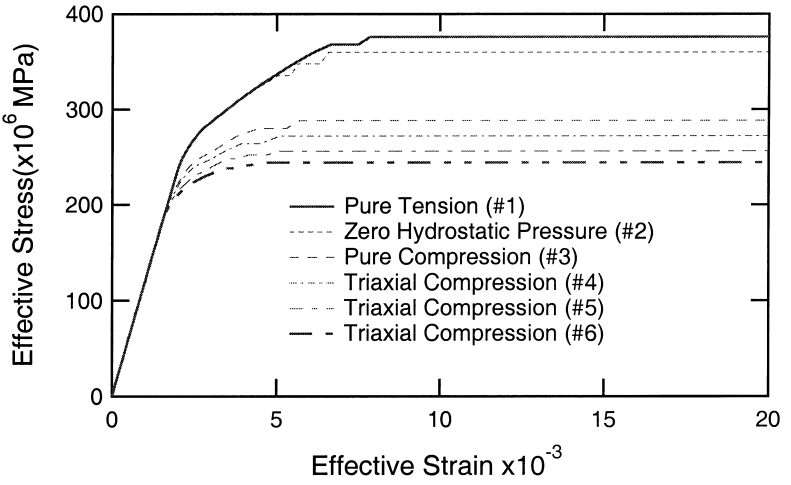

Fig. 10. Model predicted effective stress–strain plots for a polycrystalline CuZnAl SMA specimen at about $(M_s + A_s)/2$. Each one of the curves corresponds to a 1D or 3D loading.

transformation stresses will be low and as those grains transform, the cascading effect described earlier will cause an overall lower transformation level.

Before we compare the ordering of the curves between experimental and model, i.e. the trend of the transformation stress level with increasing hydrostatic pressure, first examine how the lattice parameters (or composition of SMAs) play an important

role in model results. Fig. 11 shows the trend of the transformation stress level with increasing hydrostatic pressure for both CuZnAl alloys. Although the composition of the two model materials are similar (Fig. 12), there are dramatic differences in the trend of transformation stresses for the different loading cases. The experimental results (Fig. 9) show that the effective transformation stress gently increases with increasing hydrostatic pressure, with pure compression as an exception having the highest value. This experimental result is opposite to what one would expect from a continuum analysis in which increasing hydrostatic pressure would raise the transformation stress for materials with positive volume change and lower it for materials with negative volume change. Comparing Figs. 9 and 11, although there are significant discrepancies, the response for the $Cu_{70}Zn_{26}Al_4$ material is closer to the experimental response, which is encouraging since it is the model material closer in composition to the experimental material. The counterintuitive experimental results were explained by a combination of hydrostatic effects (volume change) and crystallographic effects (number of transformation variants). The latter was inferred by a simple micromechanics model which did not account for interaction between variants; no experimental observation of variants formed was available. The simple micromechanics model predicted that more variants were available for transformation in tension than in compression and that this difference in "available variants" as a function of loading state contributed to the transformation stress levels. The conclusion was that for this material, under the given loading conditions, the crystallographic effects dominated the hydrostatic effects.

Our model predictions also show that hydrostatic effects are nearly overshadowed for tension and zero hydrostatic pressure cases for the $Cu_{70}Zn_{26}Al_4$ material. We believe the essential feature contributing to the discrepancy between results is based

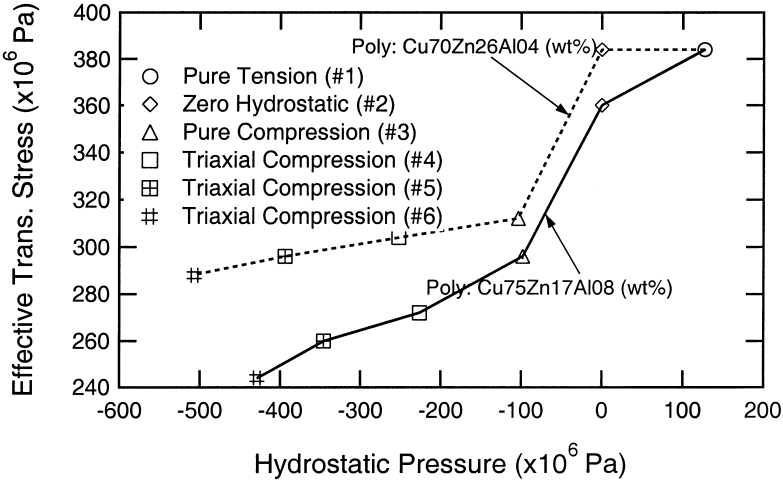

Fig. 11. Model predicted effective stress at 100% transformation vs. the hydrostatic stress at 100% transformation for a polycrystalline CuZnAl SMA specimen at about $(M_s + A_s)/2$. Each number corresponds to a 1D or 3D loading.

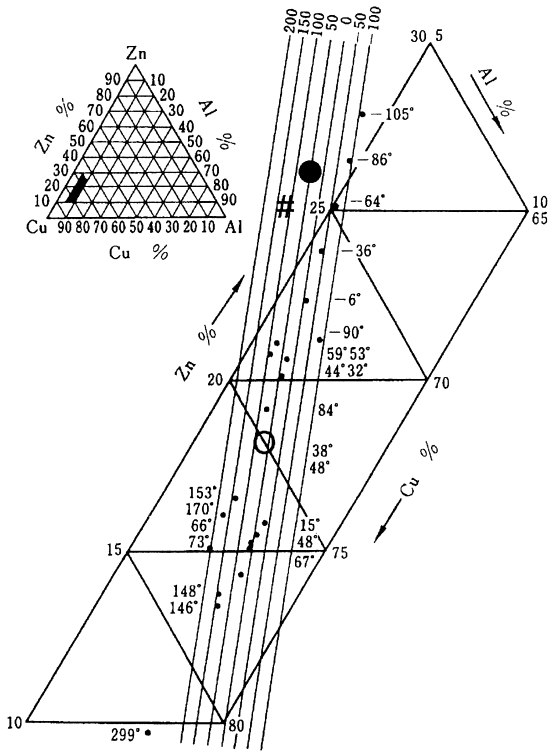

Fig. 12. A typical composition range for CuZnAl SMAs (after Delaey et al., 1978) showing the composition difference between the experimental specimen and model specimen (#, experimental, $Cu_{71}Zn_{25}Al_4$ wt.%; ●, model, $Cu_{70}Zn_{26}Al_4$ wt.%; ○, model, $Cu_{75}Zn_{17}Al_8$ wt.%).

in the crystallography: although $Cu_{70}Zn_{26}Al_4$ is very close to $Cu_{71}Zn_{25}Al_4$, the composition difference and other factors in the experimental alloy are enough to account for the discrepancies illustrated here.

In short, more experiments exploring the three dimensional stress state effects on martensitic SMA transformation are needed to verify modeling predictions. In particular, experiments that can identify number and types of variants formed under loading are essential. The results here indicate that direct comparison between micromechanics models and experimental results need to be performed to take our understanding and ability to describe SMA response to a reasonable level for multiaxial stress states. The experiments, the model and the result discrepancies indicate the importance of understanding and capturing features of the microscale response of the SMA even in macroscale models. While the Multivariant model has not yet captured the triaxial experimental results shown, there is good reason to believe that with proper lattice parameters and a few other modifications, such as accounting for single crystal anisotropy, the model could predict the kinds of counterintuitive results shown by the experiments. It is worth mentioning that plasticity-based SMA

models would require significant revision of the transformation criteria to account for material-based responses such as those illustrated in Figs. 9 and 11.

5. Conclusion

The multivariant single crystal model has been developed to simulate a polycrystalline SMA by using a number of randomly oriented single crystal grains via an averaging scheme. The polycrystalline simulations successfully capture basic features of a polycrystalline SMA, such as the gradual transformation, the different apparent moduli of martensite and the parent phase, and the nonlinear unloading stress-strain curve. Since the model is developed based on thermodynamic principles, crystallographic transformation data, and assumptions motivated by the physics of the material (e.g. self-accommodating groups of variants), we believe this approach to predict multi-dimensional SMA behavior is a promising one.

A detailed comparison was made between experimental data for triaxial loading of a polycrystalline SMA and model predictions. The results revealed that several features of the experimental data were not captured by the model accurately: strain hardening during transformation, magnitude of transformation stresses and ordering of transformation stresses with respect to hydrostatic load level. Simulations of two model materials of different composition strongly indicate the need to include crystallographic details in polycrystalline SMA modeling. Predictions for the model material nearest in composition to the experimental material were closer to experimental results. The first two discrepancies also indicate a need for the model to include the anisotropy of the austenite and martensite phases as changing compositions will not greatly impact the transformation stress levels.

While the results clearly indicate the need for additional work, both experimental and modeling, the need for a micromechanics based model of the type developed here is apparent. Plasticity based approaches to multidimensional SMA modeling would have difficulty capturing the range of effects here, while further modification to the crystallographic model shows promise. With continued work that provides good direct comparison between data and model with appropriate modifications, we hope the model proposed here can be used as a tool to better understand and predict SMA behavior and perhaps even be useful to aid in reformulating transformation criteria in phenomenological SMA models.

References

Auricchio, F., Taylor, R.L., 1997. Shape-memory alloys: modelling and numerical simulations of the finite-strain superplastic behavior. Computer Methods Appl. Mech. Engr. 143, 175–194.

Ball, J.M., James, R.D., 1987. Fine phase mixture as minimizers of energy. Arch. Ration. Mech. Anal. 100, 13–52.

Bekker, A., Brinson, L.C., 1997. Temperature-induced phase transformation in a shape memory alloy: phase diagram based kinetics approach. J. Mech. Phys. Solids 45, 949–988.

Birman, V., 1997. Review of mechanics of shape memory alloy structures. Appl. Mech. Reviews 50, 629–645.

Boyd, J.G., Lagoudas, D.C., 1996a. A thermodynamical constitutive model for shape memory materials. Part I. The monolithic shape memory alloy. Int. J. Plast. 12 (6), 805–842.

Boyd, J.G., Lagoudas, D.C., 1996b. A thermodynamical constitutive model for shape memory materials. Part II. The SMA composite material. Int. J. Plast. 12 (7), 843–873.

Brinson, L.C., 1993. One dimensional constitutive bahavior of shape memory alloys: Thermochamical derivation with non-constant material functions. J. Intell. Mater. Syst. and Struct. 4, 229–242.

Budiansky, B., Wu, T.T., 1962. Theoretical prediction of plastic strains of polycrystals. In: Proc. Fourth U.S. National Congress of Applied Mechanics, vol. 1, pp. 1175–1185, University of California, Berkeley, California.

Chakravorty, S., Wayman, C.M., 1977. Electron microscopy of internally faulted Cu-Zn-Al martensite. Acta Metall. 25, 989–1000.

Delaey, L., Deruyttere, A., Aernoudt, N., Roos, J.R., 1978. Shape memory effect, super-elasticity and damping in Cu–Zn–Al alloys. Project No. 238, Katholieke Universiteut Leuven.

Falk, F., 1983. Ginzburg–Landau theory of static domain walls in shape memory alloys. Z. Phys. B: Condens. Matter 51, 177–185.

Fremond, M., Miyazaki, S., 1996. Shape Memory Alloys, CISM, New York.

Funakubo, H., 1987. Shape Memory Alloys, Gordon and Breach Science Publishers, New York.

Gall, K., Sehitoglu, H., Maier, H.J., Jacobus, K., 1998. Stress-induced martensitic phase transformations in polycrystalline CuZnAl shape memory alloys under different stress states. Metall. Trans. A, 29A(March), 765–773. (personal communication with author corrected stated composition to Cu71Zn25Al4).

Goo, B.C., Lexcellent, C., 1997. Micromechanics-based modeling of two-way shape memory effect of a single crystalline shape-memory alloy. Acta Mater. 45 (2), 727–737.

Graesser, E.J., Cozzarelli, F.A., 1994. A proposed three-dimensional constitutive model for shape memory alloys. J. Int. Mater. Sys. Struct. 5 (January), 78–89.

Guenin, G., Pynn, R., Jara, D.R., Delaey, L., Gobin, F.P., 1980. Lattice dynamics of Cu–Zn–Al martensite. Phys. Stat. Sol. (A) 59, 553–556.

Huang, M.S., Brinson, L.C., 1998. A multivariant model for single crystal shape memory alloy behavior. J. Mech. Phys. Solids 46 (8), 1379–1409.

Jacobus, K., Sehitoglu, H., Balzer, M., 1996. Effect of stress state on the stress-induced martensitic phase transformation in polycrystalline Ni–Ti alloy. Metall. Trans. A, 27A(October), 3066–3073.

Kröner, E., 1961. Zur Plastischen Verformung des Vielkristalls. Acta Metall. 9, 155–161.

Lagoudas, D.C., Bo, Z., Qidwai, M.A., 1996. A unified thermodynamic constitutive model for SMA and finite element analysis of active metal matrix composites. Mechanics of Composite Materials and Structures 3, 153–179.

Lexcellent, C., Goo, B.C., Sun, Q.P., Bernardini, J., 1996. Characterization, thermomechanical behavior and micromechanical-based constitutive model of shape-memory Cu–Zn–Al single crystals. Acta Mater. 44 (9), 3773–3780.

Liang, C., Rogers, C.A., 1990. One-dimensional thermomechanical constitutive relations for shape memory materials. J. Int. Mater. Sys. Struct. 1 (2), 207–234.

Lim, T.J., McDowell, D.L., 1999. Mechanicsl behavior of an Ni–Ti shape memory alloy under axial-torsional proportional and nonproportional loading. Trans. Metall. Soc. AIME 121 (1), 9–18.

Lu, Z.K., Weng, G.J., 1997. Martensitic transformation and stress-strain relations of shape-memory alloys. J. Mech. Phys. Solids 45 (11/12), 1905–1928.

Lu, Z.K., Weng, G.J., 1998. A self-consistent model for the stress–strain behavior of shape-memory alloy polycrystals. Acta Metall. 46 (15), 5423–5433.

Mura, T., 1987. Micromechanics of Defects in Solids, Kluwer Academic Publishers, Boston.

Otsuka, K., Sakamoto, H., Shimizu, K., 1979. Successive stress-induced martensitic transformation and associated transformation psedoelasticiy in Cu–Al–Ni alloys. Acta Metall. 27, 585–601.

Otsuka, K., Wayman, C.M., 1998. Shape Memory Materials, Cambridge University Press, New York.

Patoor, E., Amrani, M.E., Eberhardt, A., Berveiller, M., 1995. Determination of the origin for dissymetry observed between tensile and compression tests on shape memory alloys. J. Physique IV 5 (C2), 495–500.

Patoor, E., Eberhardt, A., Berveiller, M., 1994. Micromechanical modelling of the shape memory behavior. In: Proc. ASME International Congress and Exposition, AMD-vol. 189, 23–27, Chicago.

Saburi, T., Nenno, S., 1981. The shape memory effect and related phenomena. In: Proc. An International Conference on Solid to Solid Phase Transformations, pp. 1455–1479.

Saburi, T., Wayman, C.M., 1979. Crystallographic similarities in shape memory martensites. Acta Metall. 27, 979–995.

Saburi, T., Wayman, C.M., Takata, K., Nenno, S., 1980. The shape memory mechanism in 18R martensitic alloys. Acta. Metall. 28, 15–32.

Shaw, J.A., Kyriakides, S., 1995. Thermomechanical aspects of NiTi. J. Mech. Phys. Solids 43 (8), 1243–1281.

Sun, Q.P., Hwang, K.C., 1991. A micromechanics constitutive model of transformation plasticity with shear and dilatation effect. J. Mech. Phys. Solids 39, 507–524.

Sun, Q.P., Hwang, K.C., 1993a. Micromechanics modelling for the constitutive behavior of polycrystalline shape memory alloys — I. Derivation of general relations. J. Mech. Phys. Solids 41 (1), 1–17.

Sun, Q.P., Hwang, K.C., 1993b. Micromechanics modelling for the constitutive behavior of polycrystalline shape memory alloys — II. Study of the individual phenomena. J. Mech. Phys. Solids 41 (1), 19–33.

Vivet, A., Lexcellent, C., 1998. Micromechanical modelling for tension-compression pseudoelastic behavior of AuCd single crystals. Eur. Phys. J. AP 4, 125–132.

Zhu, W., Jiang, B., Xu, Z., 1986. Crystallography of martensitic transformation in a Cu–26Zn–4Al shape memory alloy. Acta Metall. Sinica 22 (3), 229–236.